Theory of low-temperature Hall effect in stripe-ordered cuprates

Jie Lin and A. J. Millis
Department of Physics, Columbia University, 538 West 120th Street, New York, New York 10027, USA
(Received 30 June 2008; published 9 September 2008)

We investigate the effect of static antiphase stripe order on the weak-field Hall effect of electrons on a two-dimensional square lattice with electron dispersion appropriate to the high T_c cuprates. We first consider the cases where the magnitudes of the spin-and charge-stripe potentials are smaller than or of the same order as the bandwidth of the two-dimensional electrons so that the electronic properties are not too strongly one dimensional. In a model with only spin-stripe potential, and at carrier concentrations appropriate to hole-doped cuprates, increasing the stripe scattering potential from zero leads to an increase in R_H, followed by a sign change. If the scattering amplitude is yet further increased, a second sign change occurs. The results are in semiquantitative agreement with data. In a charge-stripe-potential-only model, R_H increases as the charge-stripe scattering strength increases with no sign change occurring. In a model with both spin- and charge-stripe potentials, R_H may be enhanced or may change sign, depending on the strengths of the two scattering potentials. We also consider the case in which the magnitudes of the stripe potentials are much larger than the bandwidth, where analytical results can be obtained. In this limit, the system is quasi-one-dimensional while R_H remains finite, and its sign is determined by the carrier density and the electron band parameters.

DOI: 10.1103/PhysRevB.78.115108 PACS number(s): 74.72.Dn, 71.45.Lr, 75.47.Pq

I. INTRODUCTION

Stripe order, static or fluctuating, is argued to be an important ingredient in understanding the physics of the high-temperature superconductors[1,2] and has been shown to have implications for the Hall effect.[3] In the $YBa_2Cu_3O_{6+x}$ family, stripe order was recently used to explain[4] the small pockets observed in the quantum oscillation measurements,[5,6] and to account for the important observation[7] that an electronlike Hall resistance was observed at the dopings corresponding to the small Fermi surface pockets. In the family of materials derived from La_2CuO_4, stripe order is believed to be prevalent, being related to the "1/8 anomaly" observed in most members of this material family.[8] In the $La_{1.6-x}Nd_{0.4}Sr_xCuO_4$ (Nd-LSCO) series, static-stripe order has been shown by neutron-diffraction measurements to exist over a significant part of the temperature-doping phase diagram[9] up to Sr doping $x \approx 0.25$.

The Hall resistance of $La_{1.6-x}Nd_{0.4}Sr_xCuO_4$ systems has been studied experimentally.[10,11] It was found that, at the nominal hole doping $x=0.24$, the low-temperature Hall coefficient R_H takes the value appropriate to a two-dimensional (2D) metal with carrier (hole) density $1+x$. However, for the lower dopings $x=0.20$ and $x=0.12$, the measured R_H deviates significantly from what is expected for a conventional metal with carrier density $1+x$. At $x=0.20$, R_H, while positive, is much larger than the value expected from the conventional model. For $x=0.12$, the sign of R_H is opposite, showing an electronlike behavior. A similar issue arises in the electron-doped cuprates $Pr_{2-x}Ce_xCuO_4$ (PCCO),[12] where the Hall number is positive for doping $x>0.15$ and becomes negative for smaller dopings. In the electron-doped material, the change of sign was explained by a commensurate (π,π) spin-density wave order.[13] However, in the hole-doped materials, (π,π) ordering would not produce a sign change. In this paper, we investigate whether stripe order can account for the magnitude and the unconventional doping dependence of the Hall resistivity observed in the La/Nd-Sr-Cu-O compounds.

The rest of this paper is organized as follows. Section II defines a phenomenological model for band electrons in the presence of stripe order and summarizes the formula used to calculate the conductivities. Section III illustrates the evolution of the Fermi surface in the stripe-ordered state. Section IV discusses the effects of the charge-stripe and the spin-stripe potentials on transport properties. Section V presents the doping dependence of R_H in the spin-stripe-ordered state. Section VI discusses the Hall effect in the strong stripe potential limit. Section VII is the conclusion in which the results are summarized and discussed, and implications are outlined.

II. MODEL AND FORMALISM

We assume electrons moving on a two-dimensional square lattice of unit lattice constant with a band dispersion given by

$$\varepsilon_p = -2t(\cos p_x + \cos p_y) + 4t' \cos p_x \cos p_y - 2t''(\cos 2p_x + \cos 2p_y). \quad (1)$$

In our numerical calculations, we use the canonical values[14] $t=0.38$ eV, $t'=0.32t$, and $t''=0.5t'$. In addition, we assume that the electrons feel the effect of static "stripe" (spin- and charge-density wave) order. Because we are interested only in low-temperature transport, we neglect fluctuations and treat the order in the mean-field approximation.

We take the spin modulation to be longitudinal and to be described by the wave vector $\mathbf{Q}_s$ so that it gives rise to the scattering potential

$$\Delta_s(\mathbf{R}) = 2V \cos \mathbf{Q}_s \cdot \mathbf{R}.$$

The spatial periodicity of this potential can be obtained from the incommensurate peaks in neutron-diffraction measure-

ments. Tranquada *et al.*[15] showed that, in the Nd-LSCO series for $x \lesssim 1/8$, $\mathbf{Q}_s = \pi(1-2x,1)$ while for $x > 1/8$, the spin incommensurability is approximately doping independent with wave vector $\mathbf{Q}_s^* \approx \pi(3/4,1)$. We will be mainly interested in doping $x > 1/8$, so we fix $\mathbf{Q}_s = \mathbf{Q}_s^*$.

Charge modulations are also observed in the Nd-LSCO materials.[16] These occurs at the wave vector $\mathbf{Q}_c = 2\mathbf{Q}_s$ expected from general Landau theory arguments, which allow a term $S_Q^2 \rho_{-2Q}$ in the free energy where S_Q and ρ_{-2Q} are the spin-stripe and charge-stripe order parameters, respectively.[17] We model the effect of charge stripes by the potential,

$$\Delta_Q(\mathbf{R}) = 2V_c \cos \mathbf{Q}_c \cdot \mathbf{R},$$

and we set $\mathbf{Q}_c = 2\mathbf{Q}_s^* = \pi(1/2,0)$. We have approximated the stripe potentials as simple cosines; deviations from this form were investigated and found not to be important.[4]

These considerations lead to the following Hamiltonian:

$$H = \begin{bmatrix} \varepsilon_p & V_c & 0 & V_c & 0 & V & V & 0 \\ V_c & \varepsilon_{p+(1/2,0)\pi} & V_c & 0 & 0 & 0 & V & V \\ 0 & V_c & \varepsilon_{p+(1,0)\pi} & V_c & V & 0 & 0 & V \\ V_c & 0 & V_c & \varepsilon_{p+(3/2,0)\pi} & V & V & 0 & 0 \\ 0 & 0 & V & V & \varepsilon_{p+(1/4,1)\pi} & V_c & 0 & V_c \\ V & 0 & 0 & V & V_c & \varepsilon_{p+(3/4,1)\pi} & V_c & 0 \\ V & V & 0 & 0 & 0 & V_c & \varepsilon_{p+(5/4,1)\pi} & V_c \\ 0 & V & V & 0 & V_c & 0 & V_c & \varepsilon_{p+(7/4,1)\pi} \end{bmatrix}. \quad (2)$$

We assume that the low-temperature dc transport can be described by the Boltzmann equation. We further assume that, as is appropriate for low temperatures, the relaxation is mainly due to randomly distributed impurities with a low density, leading to a constant scattering rate, $1/2\tau$. The expressions for the longitudinal and Hall conductivities then follow from solving the Boltzmann equation with the relaxation-time approximation (for a detailed derivation, see Ref. 13). Assuming the $T \to 0$ limit can be taken, these expressions are one-dimensional (1D) integrals along the Fermi surface,

$$\sigma_{xx} = \frac{\sigma_Q}{4\pi^2} \tau \oint ds \frac{v_x(s)^2}{v_F(s)}, \quad (3)$$

$$\sigma_{yy} = \frac{\sigma_Q}{4\pi^2} \tau \oint ds \frac{v_y(s)^2}{v_F(s)}, \quad (4)$$

and

$$\sigma_{xy} = \sigma_Q \frac{B}{\Phi_0} \frac{1}{4\pi} \tau^2 \oint \mathbf{v} \times d\mathbf{v} \cdot \hat{\mathbf{z}}, \quad (5)$$

where s is the arc-length coordinate along the 2D Fermi surface, $\hat{\mathbf{z}}$ is the unit vector along the c axis, and $\mathbf{v}$ is the Fermi velocity. In these equations, $\sigma_Q = e^2/\hbar$ is the conductance quantum and $\Phi_0 = hc/2e$ is the superconducting flux quantum. The Hall coefficient $R_H = \sigma_{xy}/(B\sigma_{xx}\sigma_{yy}) = 1/nec$. Here n has the meaning of an effective electron density per unit cell per plane.

We evaluate these equations by first identifying the bands that produce Fermi-surface segments and then using a numerical search procedure to locate the Fermi surface. Typically, $\sim 10^4$ Fermi-surface points are used. We then compute the velocities at each point and evaluate the integrals by the trapezoidal rule.

III. FERMI-SURFACE EVOLUTION IN THE SPIN- AND CHARGE-STRIPE-ORDERED STATES

As shown in Ref. 4, in the mean-field stripe-ordered state, the electron Fermi surface is reconstructed from the one obtained in the band theory calculation in a complicated way. The normal-state Fermi surface for doping $x = 1/8$ is shown as the solid line in Fig. 1, along with its translations by $\mathbf{Q}_s = \pi(\frac{3}{4},1)$ (dashed line) and by $(2\pi,2\pi) - \mathbf{Q}_s = \pi(\frac{5}{4},1)$ (dashed-dotted line). For small V and/or V_c, reconstruction happens in the vicinity of the hot spots (shown as solid points in Fig. 1) where the Fermi surface crosses itself upon translation by the stripe wave vectors. In Fig. 1, we only show two values of the stripe wave vectors for simplicity. The complete Fermi-surface crossing can be found in Ref. 4.

The Fermi-surface evolution in the absence of the charge-stripe potential is illustrated in Fig. 2, where the Fermi surfaces are plotted from left to right for increasing values of V. We see from Fig. 2(a) that, at relatively small V, there are well-defined hole pockets centered at $(\pm\pi/8,\pi/2)$, electron pocket centered at $(0,\pi)$, and open Fermi surface. When V is increased further, the hole pockets are eliminated [Fig. 2(b)] and at a still larger V, the electron pocket is eliminated, leaving the open Fermi surface alone [Fig. 2(c)].

The Fermi-surface evolution due to a charge-stripe potential in the absence of the spin-stripe potential is plotted in Fig. 3. We see that for the two V_c values shown here, the Fermi surface is open with no pockets.

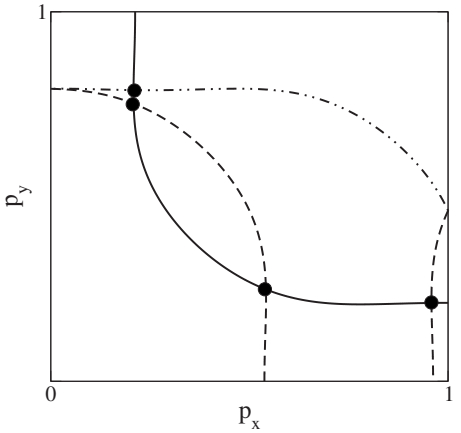

FIG. 1. The normal-state Fermi surface (solid line) for doping $x=1/8$, and its translations by $\mathbf{Q}_s=\pi(3/4,1)$ (dashed line) and by $(2\pi,2\pi)-\mathbf{Q}_s=\pi(5/4,1)$ (dashed-dotted line) in the first quadrant of the first Brillouin zone. The four hot spots are shown here as solid points. In this and the following Fermi-surface plots, the unit of momentum p is π/a with $a=1$ as the lattice constant of the square lattice.

When both types of stripe potentials are present, the Fermi-surface reconstruction is more complicated. One representative Fermi surface is shown in Fig. 4. In the case plotted, three bands cross the Fermi level. Two of them give open Fermi surfaces while the third one gives an electron pocket centered at (0,0).

The consecutive changes of the Fermi-surface topology upon changing the stripe potentials influence the Hall conductivity σ_{xy}, as well as the longitudinal conductivities σ_{xx} and σ_{yy}, and will be studied in the next section.

IV. HALL EFFECT: SPIN-STRIPE POTENTIAL VS CHARGE STRIPE POTENTIAL

A. Overview

In this section, we will consider the Hall effect in the spin- and/or charge-stripe potentials. Separate subsections treat different cases. We shall first consider the case where both potentials are weak, that is, the system is close to the quantum critical point from the normal state to the stripe-ordered state. Then, we consider the cases of spin-stripe potential only and charge-stripe potential only, and finally the effects of combined spin- and charge-stripe scattering. In this

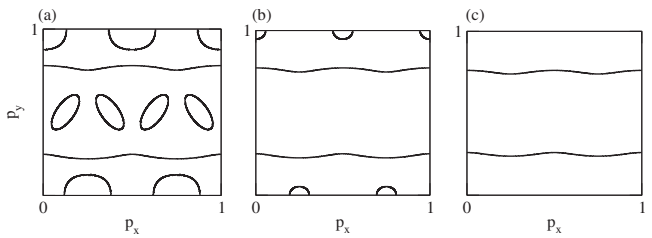

FIG. 2. Fermi-surface evolution in the spin-stripe-ordered state with the charge-stripe potential $V_c=0$ and doping $x=1/8$. (a) $V=0.2$ eV. (b) $V=0.25$ eV. (c) $V=0.3$ eV.

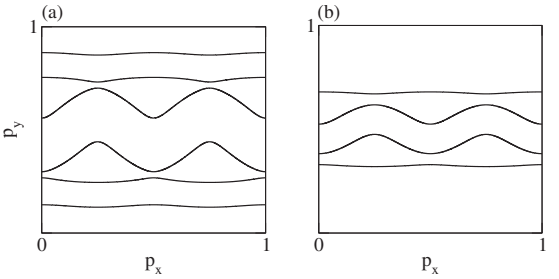

FIG. 3. Fermi surface in the charge-stripe-ordered state with the spin-stripe potential $V=0$ and a fixed doping $x=1/8$. (a) $V_c=0.15$ eV. (b) $V_c=0.35$ eV.

section, we shall fix the doping to be $x=0.125$, where the stripe order is most stable, and study the Hall effect, changing the strength of the stripe potentials V and V_c. In Sec. V, we treat the doping dependence.

B. Critical behavior close to the stripe order quantum phase transition

At small V and/or V_c, the Fermi surface reconstructs in the vicinity of the hot spots; it is essentially unchanged far from those points. Thus, although there are several Fermi-surface crossings due to the 8×8 matrix structure of H, the total changes in σ_{xy}, σ_{xx}, and σ_{yy} are additive. For each Fermi-surface crossing, our previous analysis[13] applies. We find $\delta\sigma_{xy}$ and $\delta\sigma_{xx}+\delta\sigma_{yy}$ are both linear in V and V_c, such that as $V\to 0$ and $V_c\to 0$,

$$\frac{\delta R_H}{R_H^0}=\frac{\delta\sigma_{xy}}{\sigma_{xy}^0}-\frac{\delta\sigma_{xx}+\delta\sigma_{yy}}{\sigma_{xx}^0}=aV+bV_c, \tag{6}$$

where the superscript 0 denotes the corresponding value in the normal state, and we have used the fact that the normal state has four-fold symmetry so that $\sigma_{xx}^0=\sigma_{yy}^0$. The prefactors a and b can be determined; $a\approx 6$ eV^{-1} and $b\approx 10$ eV^{-1}. In the case of PCCO,[13] this asymptotic formula holds only within 1% of the critical value. The more complicated Fermi surfaces found here will restrict the domain of validity even

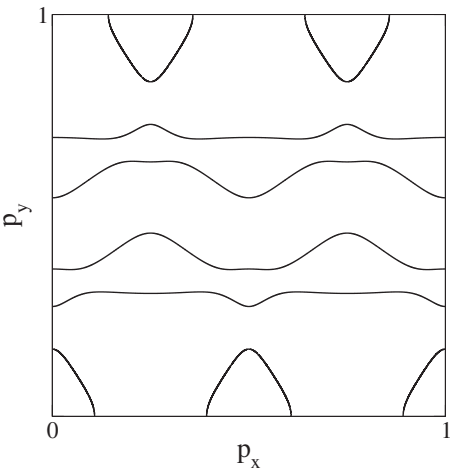

FIG. 4. The Fermi surface in the presence of both spin- and charge-stripe orders at doping $x=1/8$, $V=0.2$ eV, and $V_c=0.3$ eV.

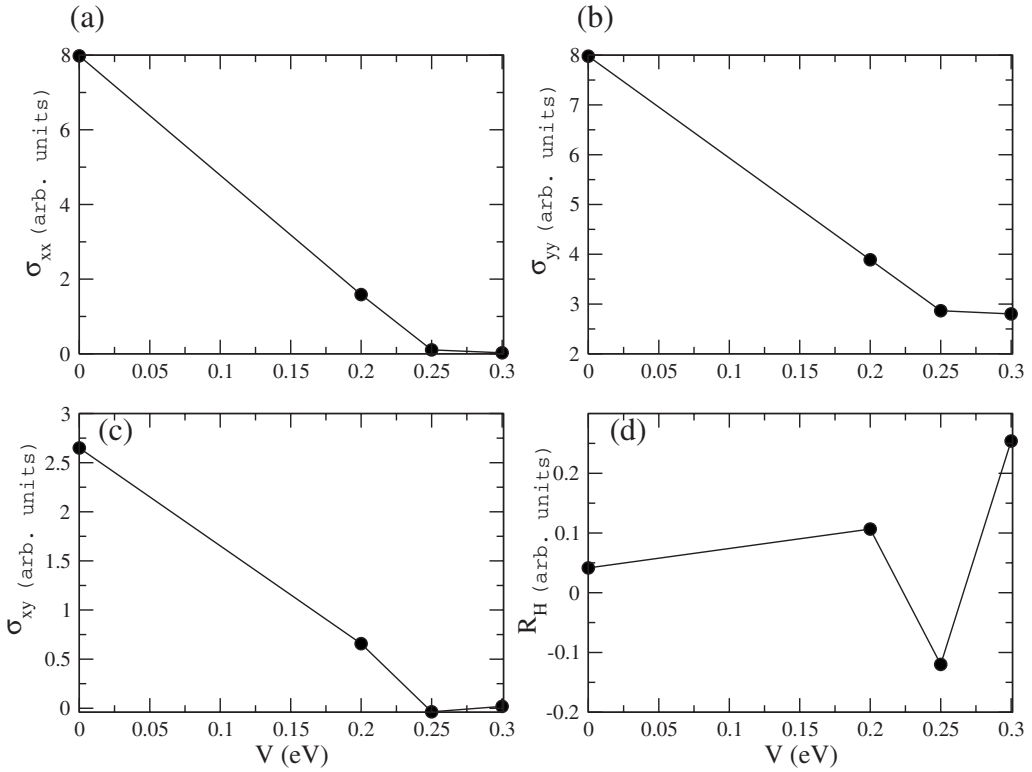

FIG. 5. Transport coefficients in the spin-stripe-ordered state at doping $x=1/8$ and $V_c=0$. (a) σ_{xx} as a function of V. (b) σ_{yy} as a function of V. (c): σ_{xy} as a function of V. (d) R_H as a function of V. Here and in the following plots of the transport properties, the solid lines are guides to the eye; exceptions will be stated explicitly.

further. For the very small values of V and V_c for which Eq. (6) applies, there are complications due to strong-field crossover[18] or magnetic breakdown.[19]

C. Spin-stripe potential only

In this subsection, we consider the case where the electrons are scattered only from the spin-stripe potential, namely, $V_c=0$. For each value of V, we calculate the loci of the Fermi surface and the Fermi velocities, and use this information in Eqs. (3)–(5). Figure 5 shows the results of such a calculation. We note that the onset of the stripe potential suppresses both the longitudinal and the Hall conductivities [Figs. 5(a)–5(c)], as in the case of the commensurate spin-density wave order in PCCO.[13] Figure 2 shows the corresponding Fermi surfaces for the three nonzero V values. We can see that the behavior of σ_{xy} can be qualitatively understood in terms of the evolution of the Fermi-surface topology.[20] For $V=0.2$ eV, R_H is positive and significantly larger than the value in the normal state. The sign is due to the dominant hole pockets [Fig. 2(a)] and the enhancement is due to the strong decrease in the longitudinal conductivities. When V grows large enough (0.25 eV here), R_H becomes negative. This reversal of sign comes from the elimination of the hole pockets [Fig. 2(b)]. The smallness of the open Fermi-surface contribution to σ_{xy} means that the electron pocket determines the sign of R_H. At still larger V (0.3 eV), the electron pocket is eliminated [Fig. 2(c)]. The open Fermi surface gives rise to a small positive contribution to σ_{xy} (holelike) so R_H becomes positive again. However, the sign of R_H due to the open Fermi surface changes as V is increased further. As will be shown in Sec. VI, the crossover to the strong-coupling limit occurs at $V\sim 1$ eV.

We notice that, in the cases with $V=0.25$ and 0.3 eV, $|R_H|$ is quite large compared to the band value $R_H(V=0)$ although σ_{xy} is much smaller than $\sigma_{xy}(V=0)$. This is due to the large anisotropy, as measured by σ_{yy}/σ_{xx}, for these two V values. This anisotropy is due to the open Fermi surfaces and grows rapidly with increasing V. This anisotropy compensates for the smallness of σ_{xy}, giving a large R_H.

Figure 5(d) shows R_H for the three values of V. We see that, as V grows, R_H first increases such that, at $V=0.2$ eV, $R_H/R_H^0\approx 2.5$ and then decreases to a negative value. This trend is qualitatively consistent with the experimental data. In the next section, we shall study the doping dependence of R_H, assuming a model in which the spin-stripe potential opens at $x=0.24$ and grows as doping is reduced. We shall see that such a model can semiquantitatively account for the experimental data.

D. Charge-stripe potential only

We now consider the effects of V_c on the transport properties with the spin potential set to zero (Fig. 6). Figure 3 shows two representative Fermi surfaces for $V_c=0.15$ eV and $V_c=0.35$ eV. For V_c in this range, all the pieces of the Fermi surface are open. However, some pieces of the open Fermi surface have relatively large curvature because they

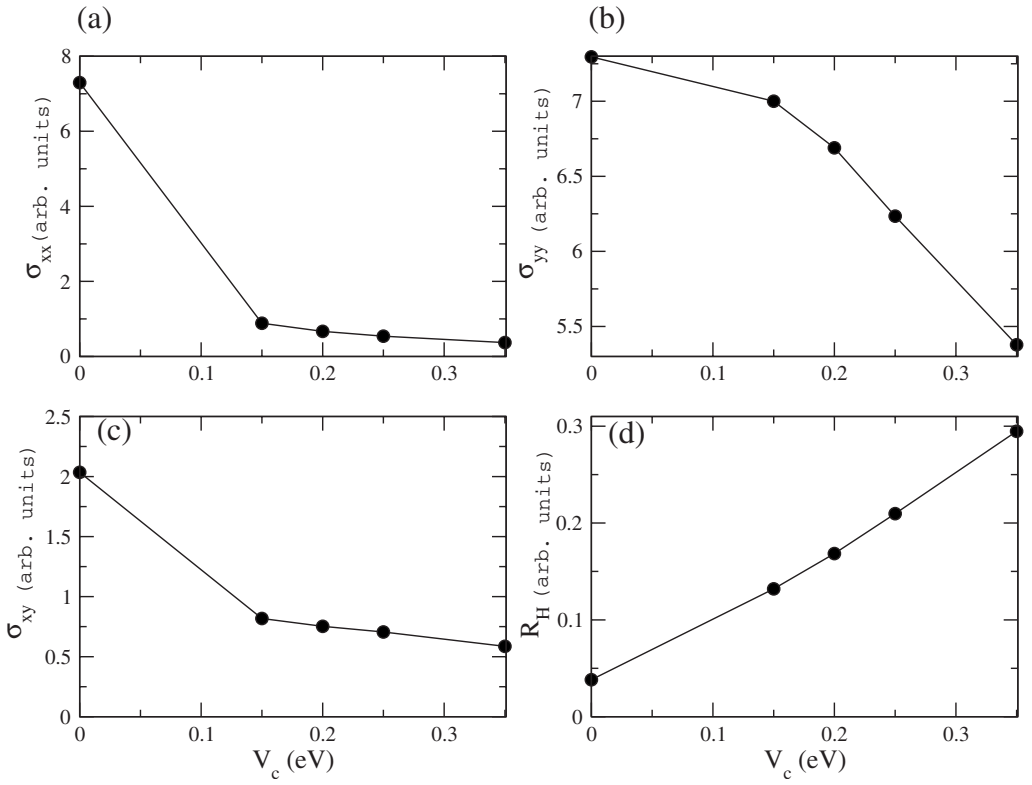

FIG. 6. Transport coefficients in the charge-stripe-ordered state calculated for doping $x=1/8$ and $V=0$. (a) σ_{xx} as a function of V_c. (b) σ_{yy} as a function of V_c. (c) σ_{xy} as a function of V_c. (d) R_H as a function of V_c.

can be viewed as the merging of the hole Fermi pockets. As shown in Fig. 6(c), σ_{xy} is thus always relatively large even for $V_c=0.35$ eV. From Fig. 6(d), we see that the onset of the charge-stripe order gives a rapid increase in R_H. In fact, $R_H(V=0,V_c=0.2\ \text{eV})=1.5R_H(V=0.2\ \text{eV},V_c=0)$. We also notice that the anisotropy is less than that in the spin-stripe case; in the spin-stripe case, $\sigma_{yy}/\sigma_{xx}\approx 100$ at $V=0.3$ eV while in the charge-stripe case, $\sigma_{yy}/\sigma_{xx}\approx 15$ at $V_c=0.35$ eV.

We see that, although the increase in the charge-stripe potential substantially enhances R_H, R_H remains positive for all the four V_c values considered here. Further calculation (not shown here) suggests that R_H changes sign around $V_c=0.8$ eV and approaches a negative value in the limit $V_c \gg t$. This suggests that a model with only charge-stripe order is inconsistent with experimental data.

E. Coexistence of the spin-stripe potential and the charge-stripe potential

Now we study the case in which the spin stripe and the charge stripe coexist, $V\neq 0$ and $V_c\neq 0$. The interplay between these two stripe potentials leads to very complicated behavior of R_H. Figure 7 shows two representative sets of results. In both cases, we fix V and increase V_c from zero to a large value. Figure 7(a) shows $R_H(V_c)$ for $V=0.2$ eV. In this case, $R_H(V_c=0)>0$, and at a small $V_c=0.05$ eV, R_H is strongly enhanced by a factor of 1.5. For $V_c=0.3$ eV, R_H becomes negative while at larger V_c, R_H is positive again. Figure 7(b) shows R_H as a function of V_c for $V=0.25$ eV. In this case, $R_H(V_c=0)<0$. At a small value of $V_c=0.05$ eV, the sign is reversed to be holelike while at larger V_c, R_H becomes negative again.

The behavior of R_H can be understood in terms of the evolution of the Fermi-surface topology when changing V_c and V. In the case of $V=0.2$ eV, for both $V_c=0.05$ eV and $V_c=0.1$ eV, the calculated Fermi surface (not shown) closely resembles that in Fig. 2(a), explaining the positive sign of R_H. For the case $V_c=0.3$ eV, the Fermi surface is given in Fig. 4 and has a qualitatively different topology such that the hole Fermi surface becomes open, and the electron pocket (which now dominates σ_{xy}) changes from being centered at $(0,\pi)$ to being centered at (0,0). At larger values of V_c, the electron pocket is eliminated, leaving open Fermi surface only, qualitatively resembling Fig. 3(b). The sign of σ_{xy} is calculated to be positive.

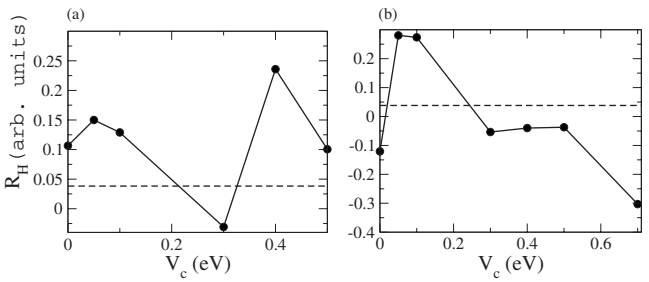

FIG. 7. R_H for nonzero V and nonzero V_c, and doping $x=1/8$. (a) $V=0.2$ eV; (b) $V=0.25$ eV. Dashed line indicates the position of R_H^0.

In the case of stronger $V=0.25$ eV, the $V_c=0$ Fermi surface is shown in Fig. 2(b). At $V_c=0.05$ eV, the hole pockets reappear with a very small radius, leading to a Fermi surface very similar to that in Fig. 2(a). However, the small hole pockets dominate the sign of R_H. The hole Fermi pockets grow with increasing V_c and eventually merge into open Fermi surface at large V_c. For $V_c=0.3$ eV, the Fermi-surface topology changes qualitatively as in the case of $V=0.2$ eV and $V_c=0.3$ eV, (Fig. 4). This Fermi-surface reconstruction can qualitatively explain the negative sign of R_H at $V_c=0.3$ eV. At $V_c=0.5$ and 0.7 eV, the electron pocket is eliminated, leaving only open Fermi surface, as qualitatively represented in Fig. 3(b). However, the sign of R_H remains negative.

The discussion in this section shows that the interplay between the spin-stripe and the charge-stripe potentials leads to two possibilities to account for the experimental observation of the sign change of R_H. In the simplest case, the spin-stripe order is dominant, and the charge-stripe order potential is small; V_c should be less than 0.05 eV when $V=0.25$ eV and $x=1/8$. Then we assume that V_c can be neglected. In the other scenario, both V and V_c are large, as shown in Fig. 7. In the next section, we pursue the first scenario in more detail.

V. HALL EFFECT: DOPING DEPENDENCE

We now study the doping dependence of the transport coefficients. Doping has two effects, changing the carrier density and changing the strength of the stripe potential. From the discussion of the last section, we assume a model for the electrons in the stripe-ordered state in which the spin-stripe scattering is dominant, and the charge-stripe scattering is neglected.

We assume a mean-field dependence of the stripe order parameter on doping for $x<0.24$,

$$V = V_0\sqrt{1 - x/0.24}, \tag{7}$$

and $V=0$ for $x>0.24$, where V_0 controls the rate at which the stripe order is setting in. Experimental results show that the $x=0.12$ sample has a negative R_H. Figure 5(d) suggests that V_0 should be relatively large, such that $0.2<V(x=0.12)<0.3$ eV. Thus, we choose $V_0=0.35$ eV. Then for each doping x, the conductivities and the Hall coefficient can be calculated from Eqs. (3)–(5). The results are shown in Fig. 8. We observe that R_H starts at $x=0.24$ ($V=0$) at the band value $1/(1+x)$, increases as doping is decreased, and jumps to a negative number around $x=0.13$.

In terms of the Fermi-surface evolution, for doping $x=0.12$, the Fermi surface can be represented by Fig. 2(b), for doping $x=0.125$, the Fermi surface resembles that in Fig. 2(a) with tiny hole pockets, and for doping in the range $0.13\leq x<0.16$, the Fermi surfaces can be represented by Fig. 2(a).

We see that R_H has a local minimum around $x=0.18$. Starting from $x=0.15$, and increasing the doping (decreasing V), R_H first decreases rapidly, and after $x\approx 0.18$, it increases and then decreases again to the band value R_H^0. This can be qualitatively understood in terms of the Fermi surface evolution. At $x=0.15$, the Fermi surface resembles that in Fig. 2(a). On increasing the doping, the size of the hole pockets centered at $(\pm\pi/8,\pi/2)$ increases. These hole pockets eventually merge into open Fermi surface [see Fig. 9(a)] for $x=0.18$. Increasing x further, additional pieces of Fermi surface appear, as shown in Fig. 9(b), which are holelike, and contribute to the increase in R_H around $x=0.2$. Because the structure of R_H in the doping range $0.15<x<0.2$ arises from the small pockets shown in Fig. 9(b), we believe it will be very sensitive to details and extrinsic effects including scattering and magnetic breakdown. On increasing the doping toward $x=0.24$ where $V=0$, R_H is then described by the critical behavior, $\delta R_H/R_H^0=aV$, with positive a.

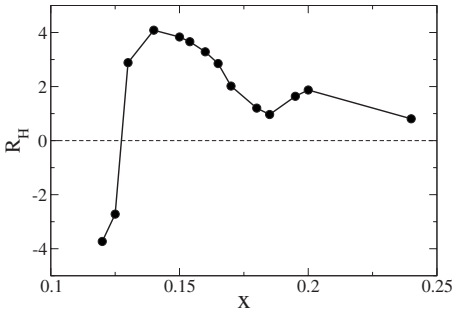

FIG. 8. R_H, expressed as the inverse of the effective carrier density per plane per cell as a function of doping. The spin-stripe potential V takes a mean-field form $V[\mathrm{eV}]=0.35\sqrt{1-x/0.24}$, and the charge-stripe potential is neglected, $V_c=0$. $R_H(x=0.24)\approx 0.8\approx 1/(1+x)$. Dashed line indicates $R_H=0$.

VI. LARGE STRIPE POTENTIAL LIMIT

In this section, we consider the case where the stripe potential $V\gg t$ and the hole doping is in the range $0.125<x<0.25$. We assume that, on average, no two electrons occupy the same lattice site. We will see that this constraint requires that $2V_c<V$. Figure 10(a) shows the spin-stripe potential for spin-up electrons. (The spin potential for spin-down electrons is opposite.)

For large spin potentials, the doped holes reside on the columns where $\Delta_s=0$ [the circles without arrows in Fig. 10(a)], referred to as charge stripes. The doped holes mainly move along these charge stripes with a small probability to hop from one stripe to another. A general Hamiltonian for charges moving in weakly coupled stripes of spacing four lattice constants is

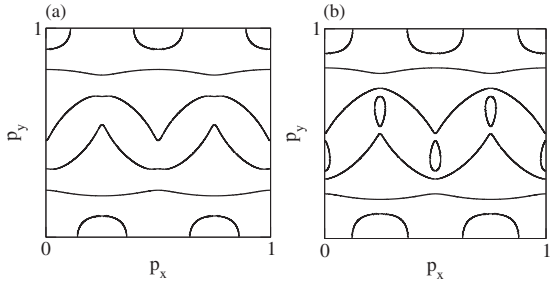

FIG. 9. Fermi surfaces for relatively small V. (a) $V=0.175$ eV, $V_c=0$, and doping $x=0.18$. (b) $V=0.143$ eV, $V_c=0$, and doping $x=0.20$.

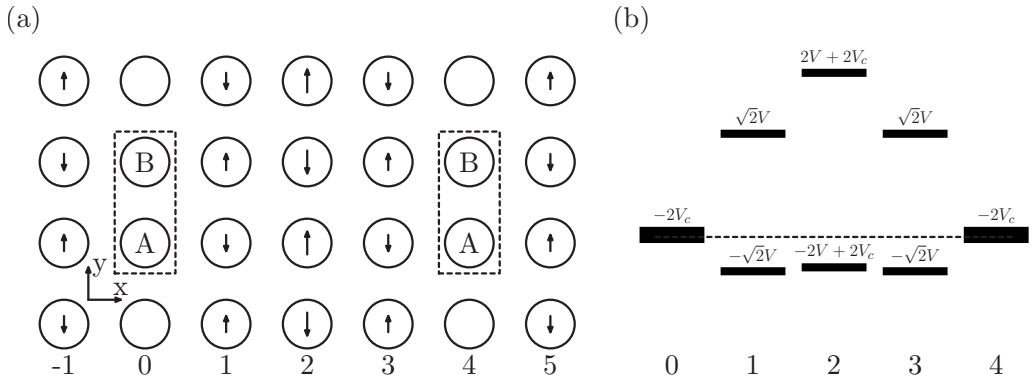

FIG. 10. (a) The spin-stripe potential for spin-up electrons. For spin-down electrons, the arrows are opposite. The length of arrows is proportional to the magnitude of the potential. The charge-stripe potential is not shown here. (b) The energy bands for each column represented by the filled boxes with height proportional to the bandwidth. In this plot, $V=3V_c$ and hole doping $x=0.125$. The Fermi level is shown as dashed line.

$$H = \varepsilon^0(p_y) + \sum_n f_n(p_y)\cos 4np_x, \tag{8}$$

with small f_n. From Eq. (5), the Hall conductivity is

$$\sigma_{xy} = -\mathcal{A}\int_{-\pi}^{\pi} dp_x v^y(p_x)\frac{dv^x(p_x)}{dp_x}, \tag{9}$$

where $\mathcal{A}=\sigma_Q\frac{B}{\Phi_0}\frac{1}{2\pi}\tau^2$. At $f_n=0$, the Fermi surface is $p_y=p_0$, and the dispersion may be approximated by

$$\varepsilon^0(p_0+\delta p_y) = v_0\delta p_y + \frac{1}{2}m_0\delta p_y^2. \tag{10}$$

To leading order in f_n, we find

$$\sigma_{xy} = -16\pi\mathcal{A}\sum_n n^2\left(\frac{m_0}{v_0} - \frac{1}{f_n}\frac{df_n}{dp_y}\right)f_n^2, \tag{11}$$

with all quantities evaluated at p_0. In most cases we find that the sign of the Hall effect is determined by the curvature of the 1D band (m_0/v_0), but for some particular parameter values, structure in the interchain hopping can produce a sign change, for example, when one of the f_n goes through zero.

The longitudinal conductivities $\sigma_{xx,yy}$ can be calculated in a similar manner in terms of f_n. To leading order of f_n, Eq. (3) can be approximated as

$$\sigma_{xx} = \mathcal{B}\int_{-\pi}^{\pi} dp_x\sqrt{1+\left(\frac{dp_y}{dp_x}\right)^2}(v^x)^2/\sqrt{(v^x)^2+(v^y)^2}$$

$$\approx \mathcal{B}\frac{16\pi}{|v_0|}\sum_n n^2 f_n^2, \tag{12}$$

where $\mathcal{B}=\sigma_Q\tau/(4\pi^2)$ and f_n is evaluated at p_0. Equation (4) can be approximated as

$$\sigma_{yy} \approx \mathcal{B}\int_{-\pi}^{\pi} dp_x|v_0| = \mathcal{B}2\pi|v_0|. \tag{13}$$

In the rest of this section, we present an evaluation of f_n in the strong-coupling limit using perturbation theory.

The zeroth order Hamiltonian describes the motion of electrons along the y direction, as defined in Fig. 10(a), in the stripe potential. The unit cell is doubled along this direction due to the spin potential, as shown by the boxes in Fig. 10(a). It is convenient to introduce a pseudospinor operator,

$$\hat{\psi}_{xy} = \begin{pmatrix} \psi_{xy}^B \\ \psi_{xy}^A \end{pmatrix}, \tag{14}$$

where x, y label unit cells as shown in Fig. 10 and $\psi_{xy}^{A,B}$ is the electron annihilation operator. Then, for the column $x=n$, the zeroth order Hamiltonian is given by

$$\mathcal{H}_n^{(0)} = \sum_{p_y} \hat{\psi}_{n,p_y}^\dagger \hat{H}_{n,p_y}^{(0)} \hat{\psi}_{n,p_y}, \tag{15}$$

with

$$\hat{H}_{n,p_y}^{(0)} = V_n^c + V_n^s\hat{\tau}_z - 2t''\cos 2p_y - t[(1+\cos 2p_y)\hat{\tau}_x - \sin 2p_y\hat{\tau}_y], \tag{16}$$

where $\hat{\tau}$'s are the Pauli matrices, and $V_0^c=-V_2^c=-2V_c$, $V_1^c=V_3^c=0$, $V_0^s=0$, $V_1^s=V_3^s=\sqrt{2}V$, and $V_2^s=-2V$. After a canonical transformation $\mathcal{T}$, which rotates the pseudospinor $\hat{\psi}$ in the pseudospin space first about the $\hat{\tau}_z$ axis by $p_y/2$ and then about the $\hat{\tau}_y$ axis by $\pi/2$, Eq. (16) becomes

$$\hat{H}_{n,p_y}^{(0)} = V_n^c + V_n^s\hat{\tau}_x - 2t''\cos 2p_y + 2t\cos p_y\hat{\tau}_z. \tag{17}$$

The energy bands on the column $n=0$ are

$$E_\pm^0 = -2V_c - 2t''\cos 2p_y \pm 2t|\cos p_y|, \tag{18}$$

with corresponding wave functions

$$|+\rangle = \begin{bmatrix} \theta(\cos p_y) \\ \theta(-\cos p_y) \end{bmatrix}, \quad |-\rangle = \begin{bmatrix} \theta(-\cos p_y) \\ \theta(\cos p_y) \end{bmatrix}. \tag{19}$$

For hole doping x in the range $0.125<x<0.25$, $\varepsilon^0(p_y)=E_-^0$. To leading order in t/V, the energy bands are $E_\pm^1=\pm\sqrt{2}V$ on the column $n=1$, $E_\pm^2=2V_c\pm 2V$ on the column $n=2$, and $E_\pm^3=\pm\sqrt{2}V$ on the column $n=3$. Figure 10(b) shows these energy bands for each column.

The motion of electrons along the x direction is described by

$$\mathcal{H}^X = \sum_{n,p_y} [\hat{\psi}^\dagger_{n+1,p_y} H^+_{p_y} \hat{\psi}_{n,p_y} + \text{h.c.}] + \sum_{n,p_y} [\hat{\psi}^\dagger_{n+2,p_y} H^{++} \hat{\psi}_{n,p_y} + \text{h.c.}], \quad (20)$$

where, after the canonical transformation $\mathcal{T}$,

$$H^+_{p_y} = -t - 2t' \cos p_y \hat{\tau}_z, \quad (21)$$

and

$$H^{++} = -t''. \quad (22)$$

We calculate the matrix elements for electrons (holes) to hop from one charge stripe to a nearby stripe by perturbation theory using $\mathcal{H}^X$ as a perturbation. In the following, we first consider the case where there is no charge potential, and then consider the case where the charge potential V_c is nonzero.

A. Spin-stripe potential only

In the absence of the charge potential, the leading-order terms in the matrix elements that describe electrons hopping among charge stripes are of order $1/V^2$. To this order, there are three possible processes whose matrix elements are denoted by M^A, M^B, and M^C. M^A is given by

$$M^A = \langle - | H^{++} \frac{1}{E^0_- - \hat{H}^{(0)}_{2,p_y}} H^{++} | - \rangle, \quad (23)$$

and represents the hopping between stripes $n=0$ and $n=4$ by two H^{++}. M^B, which represents the hopping between stripes $n=0$ and $n=4$ by two $H^+_{p_y}$ and one H^{++}, is given by the sum of the three terms,

$$M^B_{211} = \langle - | H^{++} \frac{1}{E^0_- - \hat{H}^{(0)}_{2,p_y}} H^+_{p_y} \frac{1}{E^{(0)}_- - \hat{H}^{(0)}_{3,p_y}} H^+_{p_y} | - \rangle, \quad (24)$$

$$M^B_{121} = \langle - | H^+_{p_y} \frac{1}{E^0_- - \hat{H}^{(0)}_{1,p_y}} H^{++} \frac{1}{E^0_- - \hat{H}^{(0)}_{3,p_y}} H^+_{p_y} | - \rangle, \quad (25)$$

and

$$M^B_{112} = \langle - | H^+_{p_y} \frac{1}{E^0_- - \hat{H}^{(0)}_{1,p_y}} H^+_{p_y} \frac{1}{E^0_- - \hat{H}^{(0)}_{2,p_y}} H^{++} | - \rangle. \quad (26)$$

M^C represents the hopping between stripes $n=0$ and $n=8$ by four H^{++}, and is given by

$$M^C = \langle - | H^{++} \frac{1}{E^0_- - \hat{H}^{(0)}_{2,p_y}} \times H^{++} | + \rangle \frac{1}{E^0_- - E^0_+} \langle + | H^{++} \frac{1}{E^0_- - \hat{H}^{(0)}_{6,p_y}} H^{++} | - \rangle, \quad (27)$$

where $V^s_6 = -V^s_2$.

To order $1/V^2$, the Hamiltonian H in Eq. (8) is

$$H = \varepsilon^0(p_y) + f_1(p_y)\cos 4p_x + f_2(p_y)\cos 8p_x, \quad (28)$$

where

$$f_1 = 2(M^A + M^B_{112} + M^B_{121} + M^B_{211}) = \frac{2tt''}{V^2}(2t' + t'')|\cos p_y| - \frac{t''}{V^2}[(1-\sqrt{2})t^2 + 4(1+\sqrt{2})t'^2 \cos^2 p_y], \quad (29)$$

$$f_2 = 2M^C = -\frac{t''^4}{8tV^2|\cos p_y|}, \quad (30)$$

and we have neglected the hopping processes in which an electron hops from a charge stripe into the region between stripes with a large potential and hops back to the same stripe. These processes give corrections to $\varepsilon^0(p_y)$ of order $1/V^2$ with no p_x dependence, and thus have no effects on R_H to leading order. Equation (28) can also be obtained from third order perturbation calculation of Eq. (2), treating ε_p as a perturbation.

Substituting Eqs. (29) and (30) into Eq. (11), we obtain the Hall conductivity σ_{xy} to leading order in $1/V$ in the large-V limit,

$$\sigma_{xy} = -\frac{16\pi\mathcal{A}}{V^4}\left[f_1^2\left(\frac{m_0}{v_0} - \frac{1}{f_1}\frac{df_1}{dp_y}\right) + 4f_2^2\left(\frac{m_0}{v_0} - \frac{1}{f_2}\frac{df_2}{dp_y}\right)\right] \equiv \frac{1}{V^4}\mathcal{S}_{xy}, \quad (31)$$

where all the quantities are evaluated at p_0, which is determined by the carrier density. Since both σ_{xx} and σ_{yy} are positive definite, the sign of R_H is determined by that of σ_{xy}. Similarly, substituting f_1 and f_2 into Eqs. (12) and (13), we obtain the leading-order terms of σ_{xx} and σ_{yy},

$$\sigma_{xx} = \frac{1}{V^4}\mathcal{B}\frac{16\pi}{|v_0|}[f_1(p_0)^2 + 4f_2(p_0)^2] \equiv \frac{1}{V^4}\mathcal{S}_{xx}, \quad (32)$$

and

$$\sigma_{yy} = \mathcal{B}2\pi|v_0| \equiv \sigma^\infty_{yy}. \quad (33)$$

So R_H approaches a constant as the stripe potential $V \to \infty$,

$$\lim_{V\to\infty} R_H = \frac{\mathcal{S}_{xy}}{\mathcal{S}_{xx}\sigma^\infty_{yy}} \equiv R^\infty_H. \quad (34)$$

We observe that $\mathcal{S}_{xy}$, $\mathcal{S}_{xx}$, σ^∞_{yy}, and R^∞_H are determined by the carrier density and the band parameters t, t', and t''. We perform numerical calculations of the conductivities $\sigma_{xx,xy,yy}$ and the Hall coefficient R_H for the spin-stripe potential V up to 10 eV, doping $x=0.125$, $V_c=0$, and the canonical values of the band parameters: $t=0.38$ eV, $t'=0.32t$, and $t''=0.5t'$. The results are shown as dots in Fig. 11, where we compare these numerical results to the corresponding $V\to\infty$ limits (solid lines). We observe that the numerical results indeed approach the expected values. There are small discrepancies, which we attribute to the errors in calculating the chemical potential and in numerically finding the Fermi surface. For

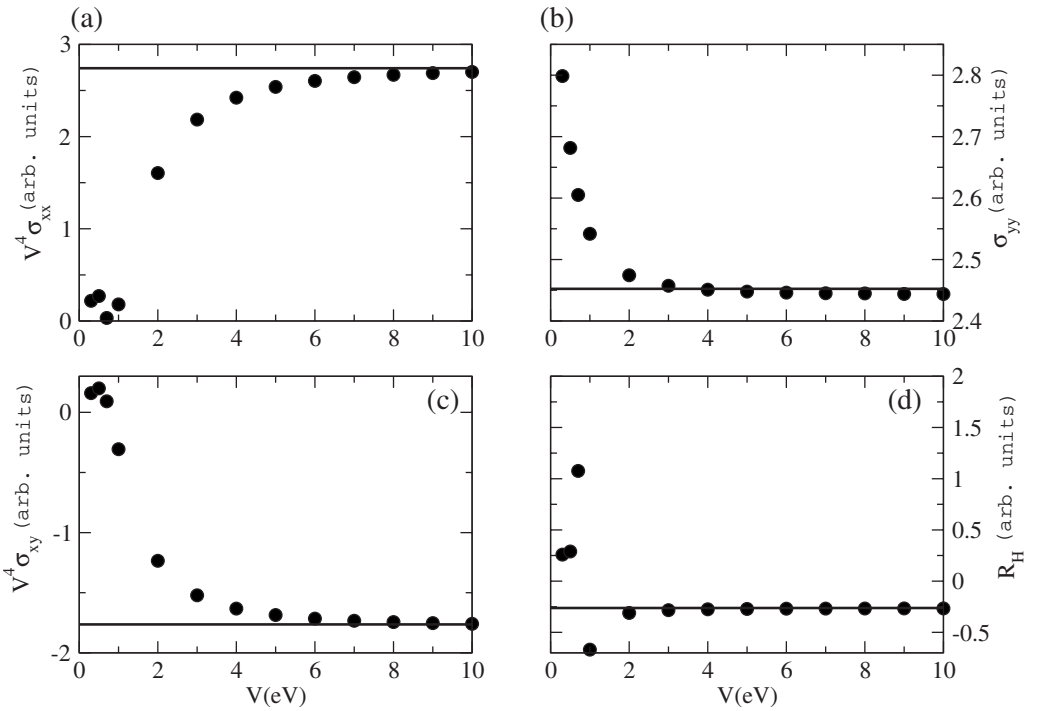

FIG. 11. Numerical results of the transport coefficients at large spin-stripe potential V, for doping $x=0.125$, $V_c=0$, and for the canonical values of t, t', and t''. (a) $V^4\sigma_{xx}$ (dots) and $\mathcal{S}_{xx}$ (solid line). (b) σ_{yy} (dots) and σ_{yy}^{∞} (solid line). (c) $V^4\sigma_{xy}$ (dots) and $\mathcal{S}_{xy}$ (solid line). (d) R_H (dots) and R_H^{∞} (solid line).

the parameters used here, $R_H^{\infty}<0$. In Sec. IV, we showed that, for $V=0.3$ eV, there is only open Fermi surface and $R_H>0$. Thus there is a change of sign in R_H for $V>0.3$ eV [roughly at $V=1$ eV, see Fig. 11(d)]. This sign change can be understood qualitatively from Eqs. (8) and (11), where we argued that σ_{xy} changes sign when one of the f_n goes through zero. We compared the Fermi surfaces for V close to 1 eV and found strong evidence that at least one of the f_n in Eq. (8) changes sign.

We now study the dependence of R_H^{∞} on doping and band parameters. Figure 12 shows R_H^{∞} as a function of doping, using the canonical values of the band parameters: $t'/t=0.32$ and $t''/t=0.16$. We also calculated R_H as a function of doping numerically for $V=10$ eV, shown as dots in Fig. 12. There is good agreement between the numerical results and R_H^{∞}. We observe that, for the canonical values of the band parameters and in the doping range $0.125<x<0.25$, R_H^{∞} <0. The sign of R_H^{∞} as a function of the band parameters t'/t and t''/t for doping $x=0.125$ is plotted in Fig. 13, which shows that the area of the gray region where $R_H^{\infty}<0$ is much larger than that of the black region where $R_H^{\infty}>0$.

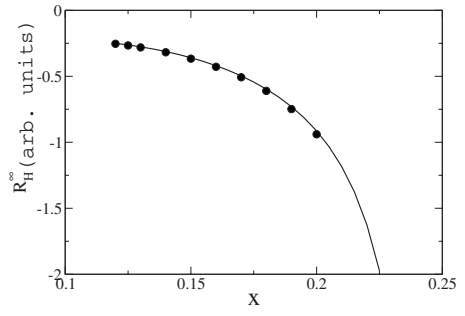

FIG. 12. R_H^{∞} as a function of doping x for $V_c=0$ and the canonical values of the band parameters. Solid line: R_H^{∞} from Eq. (34). Dots: numerical results for $V=10$ eV.

B. Coexistence of charge-stripe potential and spin-stripe potential

In this subsection, we consider the case where $V_c=\alpha V$ with $\alpha<1/2$ and $V_c \gg t$. When V_c is of the same order as V,

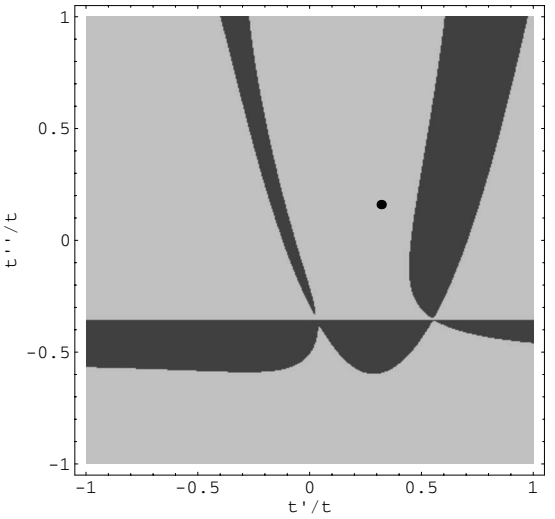

FIG. 13. The sign map of R_H^{∞}, as determined from Eq. (34), for $V_c=0$ and doping $x=0.125$. In the dark region $R_H^{\infty}>0$, and in the gray region $R_H^{\infty}<0$. The dot represents the point at $t'/t=0.32$ and $t''/t=0.16$.

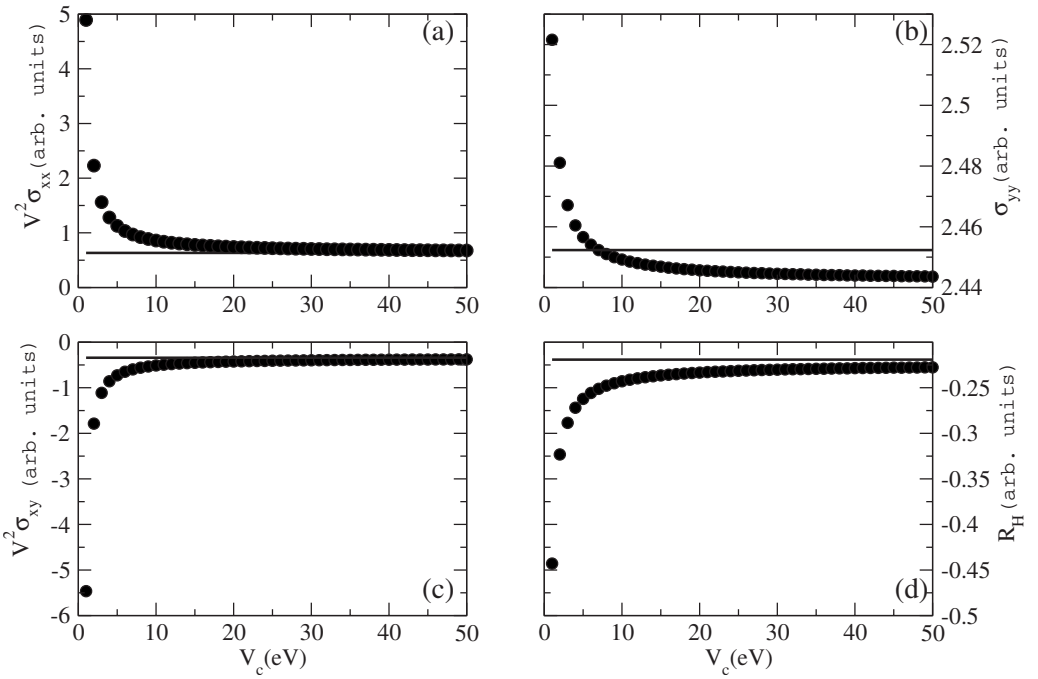

FIG. 14. Transport coefficients in the large spin- and charge-stripe potentials for $V=3V_c$, doping $x=0.125$, and the canonical values of the band parameters. (a) $V^2\sigma_{xx}$ (dots) and $\tilde{\mathcal{S}}_{xx}$ (solid line). (b) σ_{yy} (dots) and σ_{yy}^{∞} (solid line). (c) $V^2\sigma_{xy}$ (dots) and $\tilde{\mathcal{S}}_{xy}$ (solid line). (d) R_H (dots) and $\tilde{R}_H^{\infty}$ (solid line).

the leading-order term in the matrix element M^A is of order $1/V$, and it is the only term at this order. To the order of $1/V$, the Hamiltonian in Eq. (8) takes the form

$$H = -2V_c - 2t'' \cos 2p_y - 2t|\cos p_y| + \tilde{f}_1 \cos 4p_x, \quad (35)$$

where

$$\tilde{f}_1 = 2M^A = \frac{2\alpha}{1-4\alpha^2}\frac{t''^2}{V}, \quad (36)$$

and terms of order $1/V$ and independent of p_x are neglected.

Substituting Eq. (36) into Eq. (11), the Hall conductivity σ_{xy} to leading order of $1/V$ is given by

$$\sigma_{xy} = -\frac{16\pi\mathcal{A}}{V^2}\frac{m_0}{v_0}\tilde{f}_1^2 \equiv \frac{1}{V^2}\tilde{\mathcal{S}}_{xy}, \quad (37)$$

where we have used $d\tilde{f}_1/dp_y=0$. The longitudinal conductivities σ_{xx} and σ_{yy} are calculated in a similar manner, to leading order of $1/V$,

$$\sigma_{xx} = \frac{1}{V^2}\mathcal{B}\frac{16\pi}{|v_0|}\tilde{f}_1^2 \equiv \frac{1}{V^2}\tilde{\mathcal{S}}_{xx}, \quad (38)$$

and σ_{yy} is given by Eq. (33). So, R_H approaches a constant in the $V\to\infty$ limit,

$$\lim_{V\to\infty} R_H \equiv \tilde{R}_H^{\infty} = \frac{\tilde{\mathcal{S}}_{xy}}{\tilde{\mathcal{S}}_{xx}\sigma_{yy}^{\infty}} \sim -\frac{m_0}{v_0}. \quad (39)$$

We see that $\tilde{\mathcal{S}}_{xy}$, $\tilde{\mathcal{S}}_{xx}$, σ_{yy}^{∞}, and $\tilde{R}_H^{\infty}$ are determined by the ratio $\alpha=V_c/V$, the hole doping x, and the band parameters t, t', and t''. The numerical results of the conductivities $\sigma_{xx,xy,yy}$ and the Hall coefficient R_H for the charge-stripe potential V_c up to 50 eV, the spin-stripe potential $V=3V_c$, doping $x=0.125$, and the canonical values of the band parameters are shown in Fig. 14, where we compare the results to the corresponding $V\to\infty$ limits. We observe that the numerical results approach the expected values with small discrepancies that we attribute to the errors in calculating the chemical potential and in finding the Fermi surface numerically. For the parameters used here, $\tilde{R}_H^{\infty}<0$.

Equation (39) shows that $\tilde{R}_H^{\infty}$ is entirely determined by the curvature of the 1D band at p_0: m_0/v_0. We now study $\tilde{R}_H^{\infty}$ as a function of doping and the band parameters. In Fig. 15(a), we plot $\tilde{R}_H$ as a function of doping x for the canonical values of the band parameters, $t'/t=0.32$ and $t''/t=0.16$. We see that for this set of band parameters, $\tilde{R}_H^{\infty}<0$ for doping $0.125<x<0.25$ because both m_0 and v_0 are positive in this doping range. In fact, it is easy to see that $\tilde{R}_H^{\infty}<0$ in this doping range as long as $t''/t>0$. Since $\varepsilon^0(p_y)$ is independent of t', we only need to study the effects of t''/t on $\tilde{R}_H^{\infty}$. Figure 15(b) shows $\tilde{R}_H^{\infty}$ as a function of t''/t for the doping $x=0.125$. We see that $\tilde{R}_H^{\infty}<0$ for $-0.32<t''/t<0.32$.

We mention that, when the charge-stripe potential $V_c\sim t$ and $V_c \ll V$, $\tilde{f}_1$ in Eq. (36) is of the same order as f_1 in Eq. (29) and f_2 in Eq. (30). In this case, to leading order of $1/V^2$, the Hamiltonian H in Eq. (8) has the form of Eq. (28); the only difference is that the coefficient of $\cos 4p_x$ is now given by $f_1+\tilde{f}_1$. The Hall effect in this case is then similar to that in the $V_c=0$ case.

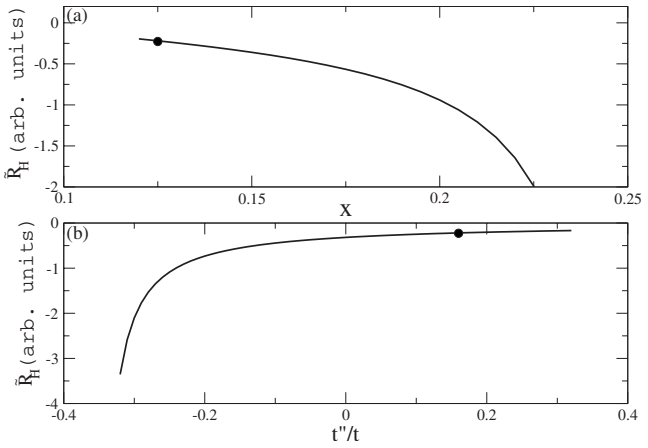

FIG. 15. (a) $\tilde{R}_H^{\infty}$ as a function of doping x for $V_c/V=1/3$ and $t''/t=0.16$. (b) $\tilde{R}_H^{\infty}$ as a function of t''/t, for $V_c=V/3$ and doping $x=0.125$. In both plots solid lines are the results from Eq. (39), and dots are from numerical calculation for $V_c=50$ eV, $V=150$ eV, doping $x=0.125$, $t'/t=0.32$, and $t''/t=0.16$.

VII. DISCUSSION

To conclude, we have considered the Hall effect in a stripe-ordered system. We found that the Hall effect R_H shows complicated behavior as the spin-stripe potential V and/or the charge-stripe potential V_c are varied. For moderate values of V and V_c, the behavior of R_H can be understood as a result of the change of the Fermi-surface topology, which is quite sensitive to the tuning of the stripe order potentials. In the strong-coupling limit, the sign of R_H was also found to depend on details.

In a model with only static spin-stripe potential V, R_H first increases from a positive band value R_H^0, then decreases to negative values, and goes back to positive values, as increasing V up to ~ 1 eV, and then has a further sign change at unphysically large V. This initial increase and the subsequent change of sign qualitatively agree with the experimental data. This is further supported from the model calculation in which V is assumed to increase when decreasing doping from $x=0.24$, as shown in Fig. 8. We mention that analogous calculations (not shown here) based on spiral order do not produce a sign change. In a model with only static charge-stripe potential V_c, our calculation shows that R_H increases from the band value until a sign change at $V_c \approx 0.8$ eV after which the sign assumes the strong-coupling limit electronlike value. This is qualitatively inconsistent with experimental data.

When both the static spin-stripe potential and the charge-stripe potential are present, R_H can be strongly enhanced or can be made negative by tuning V and V_c, as shown in Fig. 7. While both the spin-stripe model, and the V and V_c model produce a sign change in R_H, the mechanisms are different. In the spin-stripe model, the sign change of R_H is due to the electron pocket centered at $(0,\pi)$ and the elimination of the hole pockets centered at $(\pm\pi/8,\pi/2)$. In the spin- and charge-stripe model, the sign change is due to the merging of the hole pockets into open Fermi surface and the appearance of the electron pocket centered at (0,0). Measurements directly probing the Fermi surfaces are required to distinguish these two scenarios. In our calculation, we found that the open Fermi surface can give either a positive (i.e., holelike) contribution or a negative (i.e., electronlike) contribution to σ_{xy}. Under certain situations, especially when there is only open Fermi surface, this contribution, albeit small, is important since the small σ_{xx} would compensate the smallness of σ_{xy} to give a large $|R_H|$; the $V=0.3$ eV, $V_c=0$ point in Fig. 5(d), and the $V=0.25$ eV, $V_c=0.7$ eV point in Fig. 7(b), are two examples. However, once there are electron or hole pockets, the contribution to σ_{xy} from the open Fermi surface is negligible and thus the sign of R_H is fixed.

We also considered the large stripe potential limit, in which the system is quasione dimensional, and the Fermi surface is open. We showed that analytical results of R_H can be obtained in the limit $V \gg t$, both for $V \gg V_c$ and for $V > 2V_c \gg t$. In this limit, R_H depends on the carrier density, the electron band parameters, and the charge potential V_c, as previously noted by Emery and coworkers,[3] and its sign can be positive or negative.

There remain discrepancies between experiment and theory. Experiment shows that R_H at $x=0.2$ is about four times larger than that at $x=0.24$ while our calculation only shows a factor of two. However, the magnitude of R_H depends crucially on the details of the Fermi surface. Angle dependence of the scattering rate[21] (not considered here) may also be important. A systematic study of the doping dependence of the low-temperature Hall effect, as was done on PCCO,[12] would be helpful. However, the crucial generic result of our calculation is that the sign change of R_H observed in Refs. 10 and 11 appears to be strong evidence in favor of a spin-stripe order.

ACKNOWLEDGMENTS

We thank the authors of Ref. 10 for sharing their data in advance of publication and M. R. Norman for helpful discussions. This work was supported by NSF Contract No. DMR–0705847.

[1] J. Orenstein and A. J. Millis, Science **288**, 468 (2000).
[2] S. A. Kivelson, I. P. Bindloss, E. Fradkin, V. Oganesyan, J. M. Tranquada, A. Kapitulnik, and C. Howald, Rev. Mod. Phys. **75**, 1201 (2003).
[3] V. J. Emery, E. Fradkin, S. A. Kivelson, and T. C. Lubensky, Phys. Rev. Lett. **85**, 2160 (2000).
[4] A. J. Millis and M. R. Norman, Phys. Rev. B **76**, 220503(R) (2007).
[5] N. Doiron-Leyraud, C. Proust, D. LeBoeuf, J. Levallois, J.-B. Bonnemaison, R. Liang, D. A. Bonn, W. N. Hardy, and L.

Taillefer, Nature (London) **447**, 565 (2007).
[6] A. F. Bangura, J. D. Fletcher, A. Carrington, J. Levallois, M. Nardone, B. Vignolle, P. J. Heard, N. Doiron-Leyraud, D. LeBoeuf, L. Taillefer, S. Adachi, C. Proust, and N. E. Hussey, Phys. Rev. Lett. **100**, 047004 (2008).
[7] D. LeBoeuf, N. Doiron-Leyraud, J. Levallois, R. Daou, J.-B. Bonnemaison, N. E. Hussey, L. Balicas, B. J. Ramshaw, R. Liang, D. A. Bonn, W. N. Hardy, S. Adachi, C. Proust, and L. Taillefer, Nature (London) **450**, 533 (2007).
[8] A. R. Moodenbaugh, Y. Xu, M. Suenaga, T. J. Folkerts, and R. N. Shelton, Phys. Rev. B **38**, 4596 (1988).
[9] N. Ichikawa, S. Uchida, J. M. Tranquada, T. Niemöller, P. M. Gehring, S.-H. Lee, and J. R. Schneider, Phys. Rev. Lett. **85**, 1738 (2000).
[10] R. Daou, D. LeBoeuf, N. Doiron-Leyraud, S. Y. Li, F. Laliberte, O. Cyr-Choiniere, Y. J. Jo, L. Balicas, J. -Q. Yan, J. -S. Zhou, J. B. Goodenough, and L. Taillefer, arXiv:0806.2881 (unpublished).
[11] Y. Nakamura and S. Uchida, Phys. Rev. B **46**, 5841 (1992).
[12] Y. Dagan, M. M. Qazilbash, C. P. Hill, V. N. Kulkarni, and R. L. Greene, Phys. Rev. Lett. **92**, 167001 (2004).
[13] Jie Lin and A. J. Millis, Phys. Rev. B **72**, 214506 (2005).
[14] O. K. Andersen, A. I. Liechtenstein, O. Jepsen, and F. Paulsen, J. Phys. Chem. Solids **56**, 1573 (1995).
[15] J. M. Tranquada, J. D. Axe, N. Ichikawa, A. R. Moodenbaugh, Y. Nakamura, and S. Uchida, Phys. Rev. Lett. **78**, 338 (1997).
[16] J. M. Tranquada, B. J. Sternlieb, J. D. Axe, Y. Nakamura, and S. Uchida, Nature (London) **375**, 561 (1995).
[17] O. Zachar, S. A. Kivelson, and V. J. Emery, Phys. Rev. B **57**, 1422 (1998).
[18] J. Fenton and A. J. Schofield, Phys. Rev. Lett. **95**, 247201 (2005).
[19] E. I. Blount, Phys. Rev. **126**, 1636 (1962).
[20] N. P. Ong, Phys. Rev. B **43**, 193 (1991).
[21] N. E. Hussey, J. Phys.: Condens. Matter **20**, 123201 (2008).